 CMES, vol.3, no.6, pp.815-823, 2002

FE/BE Analysis of Structural Dynamics and Sound Radiation from Rolling Wheels

L. Gaul, M. Fischer[1] and U. Nackenhorst[2]

Abstract: A sequential FEM–BEM approach is employed to calculate the dynamic behavior and sound radiation of rotating wheels. The equations of motion for the wheel are developed in the frame of an Arbitrary Eulerian Lagrangian description with a time-independent formulation for steady state rolling and a spatial description of vibrations. The noise radiation caused by the vibration modes is computed by the symmetric hybrid boundary element method.

keyword: tire dynamics, finite elements, boundary elements

1 Introduction

With increasing traffic density the reduction of traffic noise becomes more and more important. Significant success in reducing sound sources in cars has been achieved. This holds for example for the main engine noise. Thus, nowadays the rolling tires are a dominating noise source and offer large potential for further reducing noise radiation from cars.

The rolling noise is mainly caused by the vibrations of the tires. These vibrations are excited by the physical contact of the rolling tires with the road surface. As a result airborne sound is generated. One step to overcome the noise problem is to optimize the tire tread design in an acoustical sense. Modern treads are designed with uneven spacing generating a broader and lower excitation spectrum. However, this technique has been tested to the extent of its limits. Further reduction techniques may include the following:

- The structural dynamic behavior of the wheel or the tires needs to be improved acoustically. In this context it has to be ensured that other important tire characteristics, including security or economical aspects will not be negatively influenced.
- The whole tire–road system needs to be optimized because the characteristic quality of the road surface implies a great potential for noise reduction as well.

Due to the complicated structure of pneumatic tires with strongly non-linear mechanical response, the exact mechanisms of all noise sources are not well understood yet. Numerical simulation methods are a promising approach to investigate the sound origins and to get more insight in the radiation mechanisms. Besides, the numerical simulation enables the observation of single design–parameter influences on the noise radiation as well as of safety and economy aspects.

Classical half-space approximations for linear-elastic rolling contact as summarised in the book by Kalkar (1990) can be used as foundation for boundary element contact formulations [Gonzalez and Abascal (2000)]. However, they come to their limits when applied to rolling tires. Therefore, in the last decade a wide range of finite element techniques were developed to simulate the structural dynamics of tires. The non-linear material behavior [Hellnwein, Liu, Meschke, and Mang (1997); Nasdala, Kaliske, Becker, and Rothert (1998)] and the dynamic effects of the rotation and the rolling contact [Faria, Oden, Yavari, Twordzydlo, Bass, and Becker (1992); Nackenhorst (1999)] are the main focus of research. The important influence of tire dynamics on the sound radiation is discussed in only few papers [Takagi and Takanari (1991), Kroop (1999)]. Nackenhorst and von Estorff (2001) give a state of the art review of numerical analysis of noise radiation from rolling tires.

Structural-acoustics problems are favorably modeled by a coupled FEM/BEM scheme. The idea was laid out by Everstine and Henderson (1990) and since then used successfully in many applications in frequency [Chen, Hof-

[1] Institut A für Mechanik, Universität Stuttgart, Pfaffenwaldring 9, 70550 Stuttgart, Germany, Email: L.Gaul@mecha.uni-stuttgart.de.
[2] Institut für Baumechanik und Numerische Mechanik, Universität Hannover, Appelstr. 9A, 30167 Hannover, Germany, Email: Nackenhorst@ibnm.uni-hannover.de.

stetter, and Mang (1998)] as well as in time domain [Lie, Yu, and Zhao (2001)]. In this paper, a new sequential FEM–BEM simulation strategy for sound radiation from rolling tires is introduced. In the first section, the computation of the dynamic behavior of rotating wheels in an Arbitrary Lagrangian Eulerian (ALE) formulation is outlined. For the description of the vibration behavior of the tire, a modal approach is employed in the configuration of steady state rolling. Following the structural section, a hybrid boundary element method for acoustics is derived. Finally, the numerical results for a simple model wheel are presented.

2 Dynamic behavior of rolling wheels

2.1 The ALE-description of rolling bodies

The dynamics of rolling bodies undergoing large elastic deflections is described efficiently by a so called Arbitrary Lagrangian Eulerian (ALE) formulation. This is the introduction of a reference configuration moving arbitrarily which is neither fixed in space nor connected to the material picture, see Fig. 1. In this special case the reference configuration describes the rigid body motion $\boldsymbol{\chi}$ of the rolling wheel, whereas $\boldsymbol{\varphi} = \hat{\phi}(\boldsymbol{\chi}, t)$ represents a mapping of the displacement field.

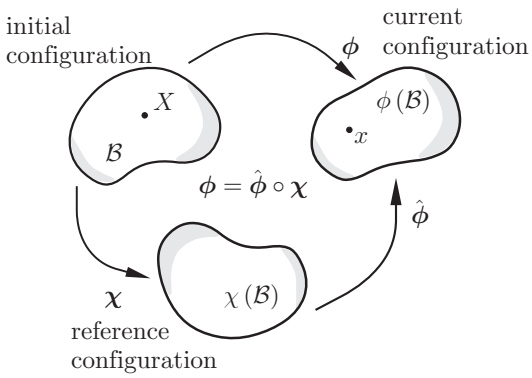

Figure 1 : ALE-Decomposition of motion.

Thus, the velocity of a material particle,

$$\boldsymbol{v}(\boldsymbol{\varphi}, t) = \hat{\boldsymbol{v}} + \boldsymbol{c} \tag{1}$$

is decomposed into the relative velocity

$$\hat{\boldsymbol{v}} := \left.\frac{\partial \boldsymbol{\varphi}}{\partial t}\right|_{\chi} \tag{2}$$

and into the convective velocity

$$\boldsymbol{c} := \mathrm{Grad}\boldsymbol{\varphi} \cdot \boldsymbol{w} \,, \tag{3}$$

where here

$$\boldsymbol{w} := \left.\frac{\partial \boldsymbol{\chi}}{\partial t}\right|_{X} \tag{4}$$

is the guiding velocity due to the rigid body motion.

In contrast to a pure Lagrangian description the following advantages result from the ALE description of rolling wheels:

- Steady state rolling is described time-independent, thus no expensive integration with respect to time has to be performed.
- The fine mesh, which is necessary for a detailed contact analysis, can be concentrated in the contact region resulting in a moderate number of unknowns.
- For adaptive mesh refinement, only the spatial discretization error has to be taken into account.
- The vibrations of rolling wheels, enforced by the tread impact and by the roughness of the road surface, are described in a spatial picture and can be immediately used as input data for the sound radiation analysis.

But nevertheless, there is a shortcoming in this formulation: Because the history of the material particles is not collected directly, special techniques for the treatment of history dependent material behavior and also the tangential contact problem with friction are required. For details it is referred to Nackenhorst (2000).

The weak form of the equations of motion is written as

$$\int_{\chi(B)} \rho \frac{\mathrm{d}\boldsymbol{v}}{\mathrm{d}t} \cdot \boldsymbol{\eta} \, \mathrm{d}v + \int_{\chi(B)} \boldsymbol{P} \cdot\cdot \mathrm{Grad}\boldsymbol{\eta} \, \mathrm{d}v = \int_{\chi(B)} \rho \boldsymbol{b} \cdot \boldsymbol{\eta} \, \mathrm{d}v + \int_{\partial_t \chi(B)} \bar{\boldsymbol{t}} \cdot \boldsymbol{\eta} \, \mathrm{d}a + \delta \int_{\partial_c \phi(B)} (p d_n + \boldsymbol{\tau} \cdot \boldsymbol{s}) \, \mathrm{d}a \,, \tag{5}$$

where the first integral describes the inertia term, with the mass density ρ measured in the reference configuration, and $\boldsymbol{\eta}$ is a test function (virtual displacement). The second integral represents the virtual work of the internal forces expressed in the reference configuration, $\boldsymbol{P}$ are

the related Piola–Kirchhoff stresses. The third and fourth integral describe the virtual work of the applied external loads, i.e. the body load density $\boldsymbol{b}$ and the surface tractions $\bar{\boldsymbol{t}}$. The contact variables are taken into account by the last term.

The inertia term in the ALE frame of reference is derived as

$$\begin{aligned}\int_{\chi(B)} \rho \frac{\mathrm{d}\boldsymbol{v}}{\mathrm{d}t}\cdot\boldsymbol{\eta}\,\mathrm{d}v &= \int_{\chi(B)} \rho\left(\left.\frac{\partial \boldsymbol{v}}{\partial t}\right|_{\chi} + \mathrm{Grad}\boldsymbol{v}\cdot\boldsymbol{w}\right)\cdot\boldsymbol{\eta}\,\mathrm{d}v \quad (6)\\ &= \int_{\chi(B)} \rho\left(\left.\frac{\partial^2\boldsymbol{\varphi}}{\partial t^2}\right|_{\chi} + 2\mathrm{Grad}\left.\frac{\partial\boldsymbol{\varphi}}{\partial t}\right|_{\chi}\cdot\boldsymbol{w}\right.\\ &\quad + \left.\mathrm{Grad}\left(\mathrm{Grad}\boldsymbol{\varphi}\cdot\boldsymbol{w}\right)\cdot\boldsymbol{w}\right)\cdot\boldsymbol{\eta}\,\mathrm{d}v\,. \quad (7)\end{aligned}$$

In this expression higher order gradients of the displacement field are present, which require special finite element techniques. But an alternative formulation can be developed by reformulation of the last term in equation (6) which leads to an almost symmetric form,

$$\begin{aligned}\int_{\chi(B)} \rho \frac{\mathrm{d}\boldsymbol{v}}{\mathrm{d}t}\cdot\boldsymbol{\eta}\,\mathrm{d}v &= \int_{\chi(B)} \rho\left(\left.\frac{\partial^2\boldsymbol{\varphi}}{\partial t^2}\right|_{\chi}\cdot\boldsymbol{\eta}\right.\\ &\quad + \boldsymbol{\eta}\cdot\mathrm{Grad}\left.\frac{\partial\boldsymbol{\varphi}}{\partial t}\right|_{\chi}\cdot\boldsymbol{w} - \left.\frac{\partial\boldsymbol{\varphi}}{\partial t}\right|_{\chi}\cdot\mathrm{Grad}\boldsymbol{\eta}\cdot\boldsymbol{w}\\ &\quad - \left.\left(\mathrm{Grad}\boldsymbol{\varphi}\cdot\boldsymbol{w}\right)\cdot\left(\mathrm{Grad}\boldsymbol{\eta}\cdot\boldsymbol{w}\right)\right)\mathrm{d}v\\ &\quad + \int_{\partial\chi(B)} \rho\,\boldsymbol{\eta}\cdot\left(\left.\frac{\partial\boldsymbol{\varphi}}{\partial t}\right|_{\chi} + \mathrm{Grad}\boldsymbol{\varphi}\cdot\boldsymbol{w}\right)\boldsymbol{w}\cdot\hat{\boldsymbol{n}}\,\mathrm{d}a\,. \quad (8)\end{aligned}$$

The first term is related to the relative acceleration and the second and third term represent the gyroscopic influence. The fourth term is due to the convective motion and the last term describes the impulse flux over the boundary. This expression vanishes identically at natural boundaries of the system, because the guiding velocity $\boldsymbol{w}$ is always perpendicular to the outward unit normal $\hat{\boldsymbol{n}}$. But it has to be taken into account, when artificial boundaries are introduced, e.g. symmetry conditions.

In the steady state case the relative velocity vanishes. Then the inertia term from Eq. (8) simplifies to

$$\begin{aligned}\int_{\chi(B)} \rho\frac{\mathrm{d}\boldsymbol{v}}{\mathrm{d}t}\cdot\boldsymbol{\eta}\,\mathrm{d}v = &- \int_{\chi(B)} \rho\left(\mathrm{Grad}\boldsymbol{\varphi}\cdot\boldsymbol{w}\right)\cdot\left(\mathrm{Grad}\boldsymbol{\eta}\cdot\boldsymbol{w}\right)\mathrm{d}v\\ &+ \int_{\partial\chi(B)} \rho\,\boldsymbol{\eta}\cdot\mathrm{Grad}\boldsymbol{\varphi}\cdot\boldsymbol{w}\boldsymbol{w}\cdot\hat{\boldsymbol{n}}\,\mathrm{d}a\,. \quad (9)\end{aligned}$$

Now, steady state rolling is described time-independent, the time derivatives are substituted by spatial gradients.

2.2 Steady state rolling

It should be mentioned that the steady state rolling case is highly nonlinear: Besides the contact problem itself, large deflections and nonlinear material behavior have to be taken into account. Therefore, an incremental iterative numerical strategy has to be involved. For simplicity we restrict ourself to an elastic–rigid contact formulation which is suitable for tire–road contact, whereas for wheel–rail contact an elastic–elastic two body theory has to be applied. For the latter case and for the formulation and computation of the rolling contact in detail it is referred to Nackenhorst (2000).

From Eq. (5) in combination with Eq. (9) by a standard approach, i.e. consistent linearization and finite element approximation,

$$\boldsymbol{\varphi} = \mathbf{N}\hat{\boldsymbol{\varphi}}\,, \quad (10)$$

the incremental finite element equations of steady state motion are obtained,

$$\left[{}^t\mathbf{K} - \mathbf{W} + \mathbf{K}_c\right]\left[\Delta\hat{\boldsymbol{\varphi}}\right] = \left[{}^{t+\Delta t}\mathbf{f}_e + {}^t\mathbf{f}_i - {}^t\mathbf{f}_\sigma - {}^t\mathbf{f}_c\right]\,, \quad (11)$$

$${}^{t+\Delta t}\hat{\boldsymbol{\varphi}} = {}^t\hat{\boldsymbol{\varphi}} + \Delta\hat{\boldsymbol{\varphi}}\,. \quad (12)$$

Herein ${}^t\mathbf{K}$ is the displacement dependent structural stiffness matrix and

$$\mathbf{W} = \int_{\chi(B)} \rho\,\mathbf{A}^T\mathbf{A}\,\mathrm{d}v \quad (13)$$

is the ALE–inertia matrix resulting from equation (9), with the matrix

$$\mathbf{A} = \begin{bmatrix} N^k_{,\iota}w_\iota & 0 & 0\\ 0 & N^k_{,\iota}w_\iota & 0\\ 0 & 0 & N^k_{,\iota}w_\iota \end{bmatrix}\,, \qquad \begin{array}{l}\text{summation over}\\ \iota = 1,2,3\,,\end{array} \quad (14)$$

which relates the convective velocity and the nodal displacements from equation (3). The matrix $\mathbf{K}_c$ is the contact tangent. The right hand side describes the equilibrium of the equivalent nodal forces, i.e. $\mathbf{f}_e$ are the externally applied loads, $\mathbf{f}_i$ are the inertia loads, $\mathbf{f}_\sigma$ represents the internal stress state and $\mathbf{f}_c$ are the contact forces. Equation (11) is solved iteratively within a Newton–Raphson scheme until the displacement rate $\Delta\hat{\boldsymbol{\varphi}}$ vanishes, i.e. the equilibrium of the nodal forces is found. The pointer t describes the iteration progress.

2.3 *Transient rolling phenomena — a modal superposition approach*

Transient vibrations of rolling tires are enforced by the tread impact and by the roughness of the road surface. From experiments it is known that in practice there is a much greater potential of noise reduction in optimizing the road–tire interface than in further optimization of the tread pattern. The tread impact leads to nonlinear reactions at least in the contact patch, and for this reason direct integration schemes have to be used. Otherwise, the wavelength of the excitation spectra from the surface roughness is very short with respect to the contact pattern, and therefore, this problem can be approximated by a superposition approach, where small vibrations $\boldsymbol{\phi}(t)$ are superimposed onto the steady state solution ${}^t\boldsymbol{\varphi}$, i.e.

$$\boldsymbol{\varphi}(t) = {}^t\boldsymbol{\varphi} + \boldsymbol{\phi}(t)$$

This behavior is modeled efficiently by modal superposition. From equation (5) in combination with equation (8), the free vibrations are described by the homogeneous finite element equation

$$\mathbf{M}\ddot{\hat{\boldsymbol{\phi}}} + \mathbf{G}\dot{\hat{\boldsymbol{\phi}}} + {}^t\mathbf{K}^*\hat{\boldsymbol{\phi}} = \mathbf{0}\,. \tag{15}$$

Herein $\mathbf{M}$ is the mass matrix and $\mathbf{G}$ is the gyroscopic matrix, which in the formulation of equation (8) reads

$$\mathbf{G} = \int_{\chi(B)} \rho\left(\mathbf{N}^T\mathbf{A} - \mathbf{A}^T\mathbf{N}\right) \mathrm{d}v\,. \tag{16}$$

The effective stiffness matrix is computed in the deformed state of steady state rolling,

$${}^t\mathbf{K}^* = \mathbf{K}({}^t\boldsymbol{\varphi}) - \mathbf{W} + \mathbf{K}_c^*({}^t\boldsymbol{\varphi})$$

where the contact conditions are frozen, which is indicated by the matrix $\mathbf{K}_c^*({}^t\boldsymbol{\varphi})$.

The corresponding eigenvalue–problem is now written as

$$\left\{\lambda_i \begin{bmatrix} \mathbf{M} & \mathbf{0} \\ \mathbf{0} & \mathbf{I} \end{bmatrix} + \begin{bmatrix} \mathbf{G} & {}^t\mathbf{K}^* \\ -\mathbf{I} & \mathbf{0} \end{bmatrix}\right\} \begin{Bmatrix} \hat{\dot{\boldsymbol{\phi}}} \\ \hat{\boldsymbol{\phi}} \end{Bmatrix} = \mathbf{0}\,. \tag{17}$$

In this context it is worth to notice, that the vibrational behavior is influenced significantly by the gyroscopic term. Due to the skew–symmetric gyroscopic matrix the eigenvectors are complex, and therefore, the vibrational behavior of rotating bodies can not be interpreted as the superposition of waves with opposite wavespeed to standing vibrations. Now the corresponding waves are traveling with different speed, where the difference is proportional to the rotating speed. It can be shown by simple experiments that this behavior is of significant influence on the sound radiated from rotating bodies, see Nackehorst (2000).

3 Hybrid boundary element method

The Hybrid Boundary Element Method (HBEM) was originally proposed by Dumont (1987) in elastostatics. For acoustics, a time-harmonic formulation of the HBEM can be derived from the Hellinger-Reissner principle. As field variable, the velocity potential $U(x,t) = \mathrm{Re}\{\hat{U}(x)\mathrm{e}^{\mathrm{j}\omega t}\}$ is introduced where only the real part of the complex ansatz has a physical meaning. Acoustic pressure and particle velocity can be obtained from the velocity potential by the relations $p = \rho\dot{U}$ and $v_i = -U_{,i}$, respectively.

The Hellinger-Reissner principle is a complementary energy functional and the derived field variable, i.e. the gradient of the velocity potential $\hat{U}_{,i}$ is considered as an independent field. On the boundary, the flux is denoted by $\hat{V} = \hat{U}_{,i}n_i$, where n_i are the components of the outward normal vector. Neumann boundary conditions are enforced in a weak sense on the section Γ_V of the boundary where the flux $\overline{\hat{V}}$ is prescribed.

The velocity potential in the domain which depends on $\hat{U}_{,i}$ is denoted by $\hat{U}^\nabla = \hat{U}^\nabla(\hat{U}_{,i})$. The velocity potential on the boundary $\hat{U}$ is interpolated independently. Compatibility of the two potential fields is achieved by weighting with a Lagrange multiplier.

With these definitions, the weak statement of the

Hellinger-Reissner functional reads

$$\int_\Omega \rho\left(\hat{U}^\nabla_{,ii}+\kappa^2\hat{U}^\nabla\right)\delta\hat{U}^{\nabla *}\mathrm{d}\Omega-\int_\Gamma \rho\left(\hat{U}-\hat{U}^\nabla\right)\delta\hat{V}^*\mathrm{d}\Gamma - \int_{\Gamma_V}\rho\left(\hat{V}-\bar{\hat{V}}\right)\delta\hat{U}^*\mathrm{d}\Gamma=0\,, \quad (18)$$

where $()^*$ denotes complex conjugate variables. The first term in Eq. (18) requires the velocity potential $\hat{U}^\nabla$ to fulfill Helmholtz equation in the domain. The following terms guarantee – as already mentioned – compatibility of the velocity potentials $\hat{U}^\nabla$ and $\hat{U}$ and Neumann boundary conditions, respectively.

For a numerical solution, proper approximation functions have to be applied. The key idea of the derivation of the HBEM is the approximation of the velocity potential field $\hat{U}^\nabla$ and the flux $\hat{V}$ by fundamental solutions $\boldsymbol{U}$ and $\boldsymbol{V}$ weighted with a generalized loads vector $\boldsymbol{\gamma}$

$$\hat{U}^\nabla(x)=\boldsymbol{U}^{\mathrm{T}}\boldsymbol{\gamma} \quad \text{and} \quad \hat{V}(x)=\boldsymbol{V}^{\mathrm{T}}\boldsymbol{\gamma}. \quad (19)$$

It should be mentioned that the HBEM is not based on a boundary integral equation and thus the field point evaluation (19) does not require a surface integration. The field $\hat{U}$ on the boundary is discretized by the product of polynomial shape functions in the matrix $\mathbf{N}$ with nodal values $\check{\mathbf{U}}$.

Modification of the domain such that small spheres with radii ε – centered at the load points collocated with the nodes where the fundamental solutions are singular – are subtracted, the modified domain Ω' with boundary Γ' is introduced. The properties of the Dirac loads acting at points located outside of the considered domain lead to a vanishing domain integral in the limit $\Omega' \to \Omega$. Inserting the approximations in the weak statement (18) yields

$$\lim_{\varepsilon\to\infty}\left\{\delta\boldsymbol{\gamma}^{\mathrm{H}}\left(\underbrace{\int_{\Gamma'}\boldsymbol{V}^*\boldsymbol{U}^{\mathrm{T}}\mathrm{d}\Gamma}_{\mathbf{F}}\boldsymbol{\gamma}-\underbrace{\int_{\Gamma'}\boldsymbol{V}^*\mathbf{N}^{\mathrm{T}}\mathrm{d}\Gamma}_{\mathbf{H}}\check{\boldsymbol{U}}\right)+\delta\check{\boldsymbol{U}}^{\mathrm{H}}\left(\underbrace{\int_{\Gamma'}\mathbf{N}^*\bar{\boldsymbol{V}}\mathrm{d}\Gamma}_{\mathbf{f}}-\underbrace{\int_{\Gamma'}\mathbf{N}^*\boldsymbol{V}^{\mathrm{T}}\mathrm{d}\Gamma}_{\mathbf{H}^{\mathrm{H}}}\boldsymbol{\gamma}\right)\right\}=0\,, \quad (20)$$

where $()^{\mathrm{H}}$ denotes the complex conjugate transpose. In contrary to Galerkin BEM methods (see for example Sirtori, Maier Novati, and Miccoli (1992)), no double surface integration is required to set up the system matrices. However, when building the matrix $\mathbf{F}$, all possible combinations of Dirichlet and Neumann load points have to be taken into account.

Applying the fundamental lemma, one can write Eq. (20) in matrix form

$$\begin{bmatrix}-\mathbf{F} & \mathbf{H}\\ \mathbf{H}^{\mathrm{H}} & \mathbf{0}\end{bmatrix}\begin{bmatrix}\boldsymbol{\gamma}\\ \check{\boldsymbol{U}}\end{bmatrix}=\begin{bmatrix}\mathbf{0}\\ \mathbf{f}\end{bmatrix}. \quad (21)$$

For further details on the hybrid boundary element method for acoustics, it is referred to the works of Wagner (2000) and Gaul, Wagner, and Wenzel (2000).

Particularly, the second equation of Eq. (21) yields

$$\boldsymbol{\gamma}=\left(\mathbf{H}^{\mathrm{H}}\right)^{-1}\mathbf{f}. \quad (22)$$

In a Neumann-problem, the vector of equivalent nodal forces $\mathbf{f}$ is given completely by the normal particle velocity $\bar{\boldsymbol{V}}$ on the boundary. Thus, by Eq. (22) the weighting parameters $\boldsymbol{\gamma}$ can be obtained and then inserted in the domain approximation Eq. (19) yielding the complete field solution. For this, only the complex conjugate transpose of the matrix $\mathbf{H}$ needs to be calculated and no further boundary integrations are necessary [Gaul, Wagner, and Wenzel (1998)].

3.1 Mirror technique for reflecting surface

For the calculation of noise radiation from rolling tires, the influence of the road impedance has to be taken into account. When – as approximation of the actual impedance boundary condition – the road surface can be modeled as hard-walled, boundary element methods offer an efficient approach: the so-called mirroring technique of the fundamental solution. This idea of using a modified Green's function is widely used in boundary element methods. In underwater acoustics, for example, the free surface and the seabed can be modeled elegantly [Santiago and Wrobel (2000)].

The fundamental solution for the Helmholtz equation in full space is given by

$$U=\frac{1}{4\pi r}e^{-ikr}. \quad (23)$$

Herein, r is the Euclidean distance between the field point $\mathbf{x}$ and the load point $\boldsymbol{\xi}$. By the use of the modified test function

$$U_h(r,r')=\frac{1}{4\pi}\left(\frac{1}{r}e^{-ikr}+\frac{1}{r'}e^{-ikr'}\right), \quad (24)$$

a hard–walled surface of the road is implemented without discretization of the road surface. r' is the distance between the field point and the mirror image of the load point on the hard–walled surface as shown in Fig. 2. The mirror technique can be visualized as a superposition of two sound fields, the actual sound field generated by the radiator and a reflected wave from the road surface. In conclusion only the surface of the tire has to be discretized. The Sommerfeld radiation condition is fulfilled a priori by the fundamental solution, thus no waves are reflected from the boundary Γ_∞ at infinity.

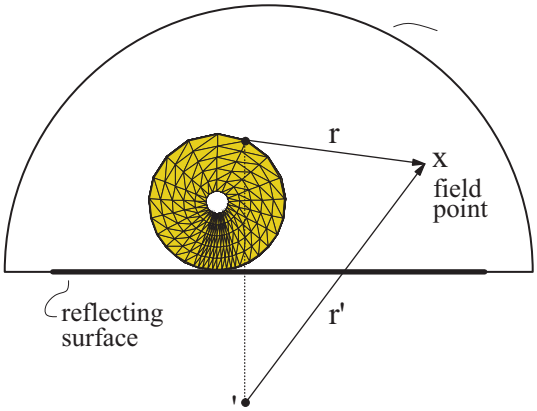

Figure 2 : Mirror technique for fundamental solution.

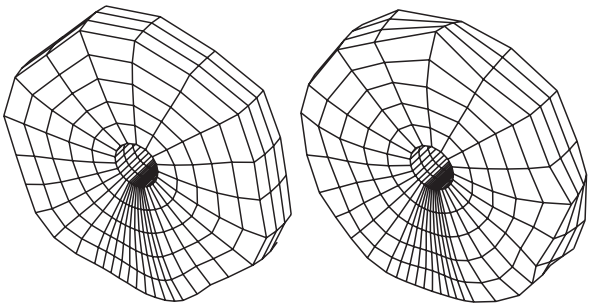

1280 Hz 1424 Hz

Figure 3 : Eigenmodes of rolling wheel.

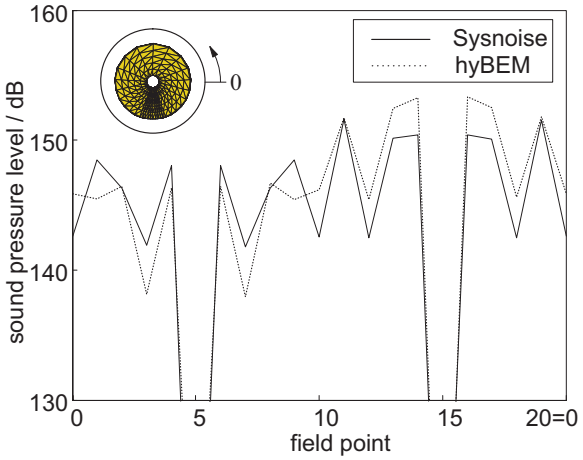

Figure 4 : Comparison of sound pressure level on field point circle ($a = 0.42m$) at 1280 Hz. Sysnoise / hyBEM.

4 Numerical example: a simple model wheel

As an example for the proposed method, the sound radiation from a simple model wheel with radius $a_0 = 0.3m$ is studied. The configuration of steady state rolling at 40 km/h is computed in the framework of the ALE formulation described in the first section. The subsequent eigenanalysis is carried out in the deformed state with frozen contact conditions under the simplification of vanishing gyroscopic terms. Fig. 3 shows two eigenmodes of the rolling wheel at 1280 Hz and 1424 Hz, respectively. Lower eigenmodes are not shown, since below a limit frequency, no far-field sound radiation occurs.

Noise radiation from the wheel is computed for each eigenmode separately. The normal velocities on the wheel surface obtained in the FEM eigenanalysis yield the Neumann boundary conditions for the acoustic domain. In this paper, sound pressure is scaled to the mass-normalized structural eigenmodes, thus the sound pressure levels do not indicate absolute values in operating conditions.

To validate the proposed hybrid boundary element method with direct evaluation of the field data, results from hyBEM and the commercial BEM code Sysnoise are compared in Fig. 4. In this example, the sound radiation from the structural eigenmode at 1280 Hz in free space is computed. Sound pressure levels are evaluated on a circle with radius $a = 0.42m$, i.e. approximately one element-length away from the surface to avoid boundary-layer effects. The results correspond nicely, with differences of about 2 dB. Both simulations predict the same very low radiation straight up or down.

From now on, all results are calculated with the boundary element code hyBEM using the HBEM and direct evaluation of field points, i.e. without building the **F** matrix and computing the unknown boundary data. Fig. 5

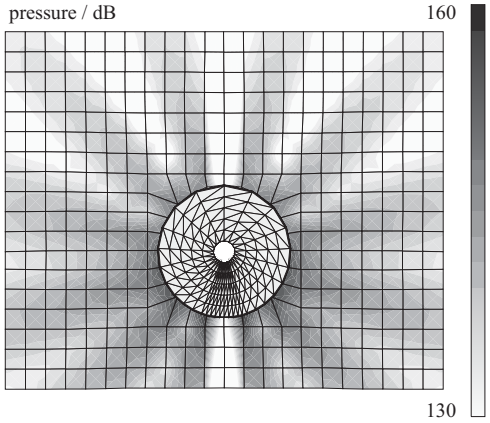

Figure 5 : Sound radiation of eigenmode at 1280 Hz in free space. hyBEM.

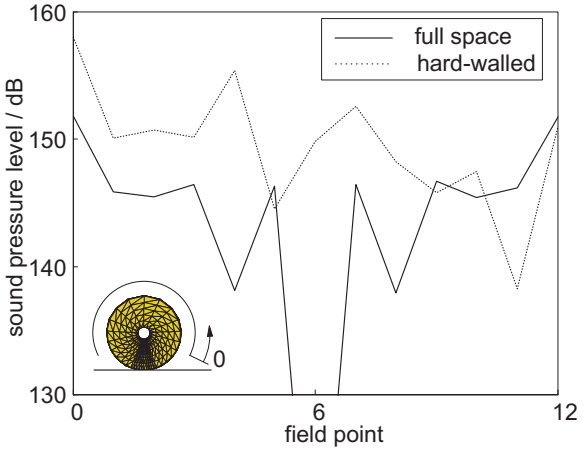

Figure 6 : Comparison of full space solution vs. model with hard-walled road surface. Sound pressure level evaluated on circle segment ($a = 0.42m$).

shows the radiated pressure pattern of the eigenmode at 1280 Hz in free space, i. e. neglecting the influence of the road surface. The plot shows the sound radiation in the plane perpendicular to the tire axis.

In the following, the influence of the road surface is modelled as hard-walled boundary using the mirror technique as described in the previous section. Fig. 6 compares the sound pressure levels evaluated on a circle segment with radius $a = 0.42m$. Taking into account the hard-walled road surface by the modified test function (24), the radiation characteristics change significantly. One notices that the overall pressure level increases slightly. However, there are points where the pressure level decreases due to the superposition of the reflected sound waves.

In Fig. 7 the radiated sound field calculated with the mirror technique is shown on the plane perpendicular to the wheel axis. One notices the changed radiation characteristic and the increase of sound pressure level compared to the full space solution in Fig. 5. The non-symmetric pressure pattern due to the rotation of the wheel is emphasized by the reflection on the hard-walled surface. The sound-radiation parallel to the wheel axis (Fig. 8) is significantly lower than the pressure level perpendicular to the wheel axis.

Next, sound radiation from another structural eigenmode at 1424 Hz is examined. Again, the road surface is modelled hard-walled. Fig. 9 and Fig. 10 show the sound pressure level pattern on planes perpendicular and parallel to the wheel axis, respectively. The sound radiation parallel to the axis is dominating the mode at 1424 Hz.

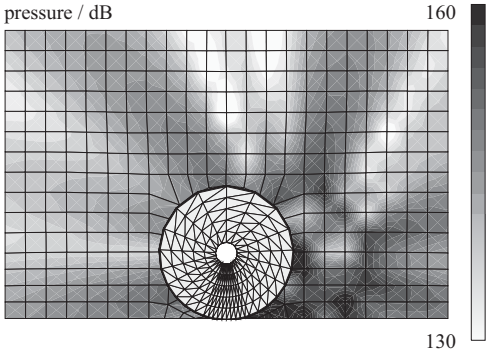

Figure 7 : Sound radiation of eigenmode at 1280 Hz. Road surface is modelled hard-walled using mirror technique.

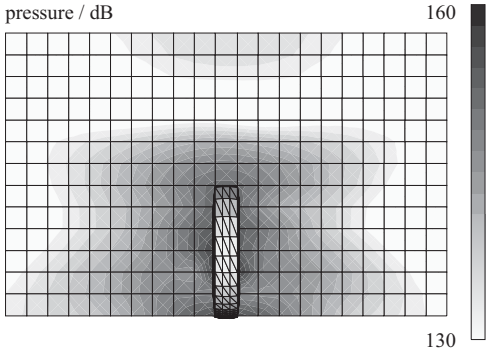

Figure 8 : Sound radiation of eigenmode at 1280 Hz. Hard-walled surface. Plane parallel to wheel axis.

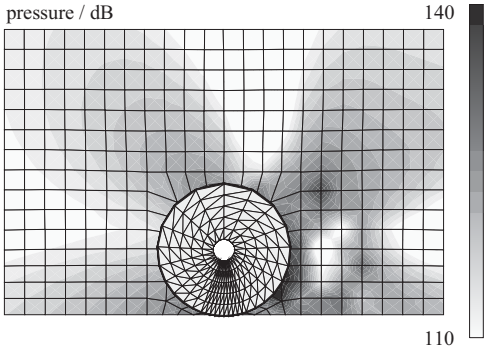

Figure 9 : Sound radiation of eigenmode at 1424 Hz. Hard-walled surface. Plane perpendicular to wheel axis.

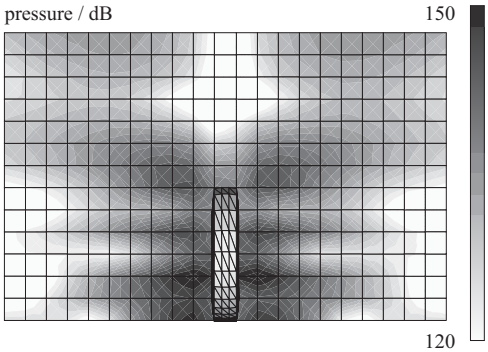

Figure 10 : Sound radiation of eigenmode at 1424 Hz. Hard-walled surface. Plane parallel to wheel axis.

The pressure in the plane perpendicular to the wheel axis is one order of magnitude below the values that were calculated for the structural eigenmode at 1280 Hz.

5 Conclusions

Based on eigenmodes, which are determined in the deformed state of a stationary rolling wheel by finite element techniques, sound radiation analysis is carried out by the hybrid boundary element method. This allows the simulation of the radiation characteristics of single mode shapes.

The ALE description of the dynamics of the rolling wheel allows the time-independent description of steady state rolling. An eigenanalysis in this frozen configuration yields directly the input data for the HBEM computation of noise radiation from the rolling tire. For acoustic far-field problems, boundary element formulations offer the advantage that the problem dimension is reduced by one and the Sommerfeld radiation condition is fulfilled inherently. Furthermore, a hard–walled road surface can be modeled by mirroring technique without discretization. For the Neumann problem of sound radiation from a tire, the HBEM in particular allows a numerically very efficient field point evaluation.

References

Chen, Z. S.; Hofstetter, G.; Mang, H.A. (1998): A Galerkin-type BE-FE formulation for elasto-acoustic coupling. *Computer Methods in Applied Mechanics and Engineering*, vol. 152, pp.1478-155.

Dumont, N. A. (1987): The hybrid boundary element method. In Brebbia, C.A.; Wendland, W.; Kuhn, G. (Eds): *Boundary Element IX*. Computational Mechanics Publications, Southampton.

Everstine, G. C.; Henderson, F. M. (1990): Coupled finite element/boundary element approach for fluid structure interaction. *Journal of the Acoustical Society of America*, vol 87, no. 5, pp. 1938-1947.

Faria, L. O.; Oden, J. T.; Yavari, B.; Tworzydlo, W. W.; Bass, J. R.; Becker, E. B. (1992): Tire modeling by finite elements. *Tire Science & Technology*, vol. 20, no. 1, pp. 33-56.

Gaul, L.; Wagner, M.; Wenzel, W. (1998): Efficient field point evaluation by combined direct and hybrid boundary element methods. *Engineering Analysis with Boundary Element Methods*, vol. 21, pp. 215-222.

Gaul, L.; Wagner, M.; Wenzel, W. (2000): Hybrid boundary element methods in frequency and time domain. In von Estoff, O. (Ed): *Boundary Elements in Acoustics*, pp. 121-163. WIT Press, Southampton.

Gonzalez, J.A.; Abascal, R. (2000): Solving rolling contact problems using boundary element method and mathmatical programming algorithms. *CMES: Computer Modeling in Engineering & Sciences*, vol. 1, no. 3, pp. 141-150.

Hellnwein, P.; Liu, C. H.; Meschke, G.; Mang, H. A. (1997): A new 3-d finite element model for cord-reinforced rubber composities – applications to analysis of automobile tires. *Finite Elements in Analysis and Design*, vol. 14, pp. 1-16.

Kalkar, J. J. (1990): *Three-dimensional Elastic Bodies in Rolling Contact.* Kluwer Academic PRess, Dordrecht, The Netherlands.

Kroop, W. (1999): A mathmatical model of tire noise generation. *Heavy Vehicle Systems*, vol. 6, pp. 310-329.

Lie, S. T.; Yu, G.; Zhao, Z. (2001): Coupling of BEM/FEM for time domain structural-acoustic interaction problems. *CMES: Computer Modeling in Engineering & Sciences* vol. 2, no. 2, pp. 171-182.

Nackenhorst, U. (1999): A new finite element rolling contact algorithm. In Brebbia, C.; Gaul, L.(Eds): *Computational Methods in Contact Mechanics IV.* Compuational Mechanics Publications, Southhampton.

Nackenhorst, U. (2000): *Rollkontaktdynamik – Numerische Analyse der Dynamik rollender Körper mit der Finite Elemente Methode*. Hablilitation thesis, University of the Federal Armed Forces, Hamburg.

Nackenhost, U.; von Estorff, O. (2001): Numerical analysis of tire rolling noise radiation – a state of the art review. In *Proceedings of Inter-Noise 2001*, The Hague, The Netherlands.

Nasdala, L.; Kaliske, M.; Becker A.; Rothert, H. (1998): An efficient viscoelastic formulation for steady state rolling. *Compuational Mechanics*, vol. 22, pp. 395-403.

Santiago, J. A. F.; Wrobel, L. C. (2000): A boundary element model for underwater acoustics in shallow water, *CMES: Computational Modeling in Engineering & Sciences*, vol. 1, no. 3, pp. 73-80.

Sirotori, S.; Maier, G.; Novati, G.; Miccoli, S. (1992): Agalerkin symmetric boundary element method in elasticity: formulation and implementation. *International Journal for Numerical Methods in Engineering*, vol. 35, pp. 255-282.

Takagi, R.; Takanari, S. (1991): Tire structural parameter analysis for road noise using an accurate FEM model. *SAE Transactions*, vol. 100, no. 5, pp. 987-996.

Wagner, M. (2000): *Die hybride Randelementmethode in der Akustik und zur Struktur-Fluid-Interaktion.* PhD thesis, University of Stuttgart.